Drosophila ventral furrow morphogenesis: a proteomic analysis

Lei Gong*, Mamta Puri*, Mustafa Ünlü†, Margaret Young, Katherine Robertson, Surya Viswanathan, Arun Krishnaswamy, Susan R. Dowd and Jonathan S. Minden‡

Department of Biological Sciences and The NSF Science and Technology Center for Light Microscope Imaging and Biotechnology, Carnegie Mellon University, Pittsburgh, PA 15213, USA

*These authors contributed equally to this work
†Present address: Millennium Pharmaceuticals, Cambridge, MA 02319, USA
‡Author for correspondence (e-mail: minden@cmu.edu)

Accepted 30 October 2003

Development 131, 643-656
Published by The Company of Biologists 2004
doi:10.1242/dev.00955

Summary

Ventral furrow formation is a key morphogenetic event during *Drosophila* gastrulation that leads to the internalization of mesodermal precursors. While genetic analysis has revealed the genes involved in the specification of ventral furrow cells, few of the structural proteins that act as mediators of ventral cell behavior have been identified. A comparative proteomics approach employing difference gel electrophoresis was used to identify more than fifty proteins with altered abundance levels or isoform changes in ventralized versus lateralized embryos. Curiously, the majority of protein differences between these embryos appeared well before gastrulation, only a few protein changes coincided with gastrulation, suggesting that the ventral cells are primed for cell shape change. Three proteasome subunits were found to differ between ventralized and lateralized embryos. RNAi knockdown of these proteasome subunits and time-dependent difference-proteins caused ventral furrow defects, validating the role of these proteins in ventral furrow morphogenesis.

Key words: *Drosophila*, Gastrulation, Ventral furrow formation, Proteomics

Introduction

Drosophila gastrulation involves four major morphogenetic events: ventral furrow formation, posterior-midgut invagination, cephalic furrow formation and germband extension (Costa et al., 1993). The first three morphogenetic events are driven by cell shape changes; while germband extension is driven by cell intercalation. The first morphogenetic change is ventral furrow formation, which leads to the internalization of mesodermal precursors. This process begins stochastically by a flattening of the apical membranes of a 10- to 12-cell wide central patch of ventral cells (Kam et al., 1991; Sweeton et al., 1991). The nuclei of these cells then lose their apical attachment and migrate basally. This is followed by an apical constriction and shortening along the apical/basal axis, which converts the columnar-shaped cells into wedge-shaped cells. About half of the cells in the central patch undergo these shape changes over a 10- to 12-minute period. This is sufficient for the entire ventral furrow to collapse inward, bringing a band, four cells wide on either side of the central patch, into the interior of the embryo over a period of several minutes. Cytoplasmic myosin relocates from the basal to the apical side of the cell during invagination (Young et al., 1991; St. Johnston and Nüsslein-Volhard, 1992). Once in the interior of the embryo, the mesodermal cells adopt a mesenchymal shape, disperse, and migrate along the inner surface of the epidermal cell layer.

Ventral furrow cells are specified by a signaling cascade that activates the ubiquitously distributed transmembrane receptor protein, Toll on the ventral side of the embryo (Thisse et al., 1988). Toll signaling results in the dissociation of the cytoplasmic heterodimer of Dorsal and Cactus, which are homologs of NFκB and IκB, respectively. Free Dorsal, which is a member of the rel family of transcription factors, migrates into the nucleus where it activates the transcription of *twist* (*twi*), which encodes a basic helix-loop-helix protein (Boulay et al., 1987). Twist and Dorsal act cooperatively to activate the transcription of *snail* (*sna*), which encodes a zinc-finger transcriptional regulator (González-Crespo and Levine, 1993; Leptin and Grunewald, 1990; Leptin, 1991). Embryos mutant in *twi* or *sna* fail to form proper ventral furrows (St. Johnston and Nüsslein-Volhard, 1992). *twi* mutant embryos are capable of eventually forming a shallow, narrow furrow. Transverse sections of *twi* embryos show that the ventral cells release their nuclei, but fail to constrict their apical membranes and shorten. *sna* mutant embryos form a weaker furrow that is very shallow and wavy. The ventral cells of *sna* embryos fail to release their nuclei from the apical surface, which appears to inhibit apical constriction, but they are capable of cell shortening. Embryos doubly mutant for *twi* and *sna* fail to form a ventral furrow of any kind. Thus it appears that *twi* and *sna* control separate processes and these processes occur independently.

Two other genes known to be required for proper furrow formation are *folded gastrulation* and *concertina* (Costa et al., 1994; Parks and Wieschaus, 1991). Embryos mutant for either gene form a ventral furrow, but in an uncoordinated and delayed fashion. *folded gastrulation* and *concertina* are also essential for posterior-midgut invagination. Concertina is a maternally supplied Gα homologue that is uniformly distributed throughout the embryo, while *folded gastrulation* encodes a novel secreted protein that is expressed zygotically

in a ventral pattern. It is thought that these proteins are part of a signaling pathway that is required for the coordination of the ventral furrow cell shape changes. A germline mutant screen identified a role for DRhoGEF2 in ventral furrow formation (Chou and Perrimon, 1996; Perrimon et al., 1996). DRhoGEF stimulates the small GTPase, Rho, to exchange its bound GDP for GTP, thereby activating Rho. A dominant negative form of Rho also produces ventral furrow defects. In tissue culture cells, Rho has been shown to stimulate stress fiber formation (Hall, 1998). These results indicate that the actin cytoskeleton is involved in ventral furrow formation. However, the precise role of Rho and RhoGEF in ventral furrow morphogenesis is still unknown.

Ventral furrow morphogenesis is a complex process that encompasses many different cellular functions, such as: signal transduction, transcriptional regulation and cytoskeletal rearrangements. Recently, mutations in *tribbles* and *frühstart*, were found to have ventral furrow defects because the ventral cells entered mitosis prematurely (Mata et al., 2000; Grosshans and Wieschaus, 2000; Seher and Leptin, 2000). Thus, cell cycle control is also part of the cellular processes that distinguish ventral cells from their neighbors.

We have taken a comparative proteomics approach to identify additional proteins that make ventral furrow cells different from adjacent lateral cells. There are several thousand protein species in *Drosophila* embryonic cells (Santaren, 1990). We presume that the vast majority of proteins are common to both ventral and lateral cells and that the difference between these cells lies in a relatively small number of proteins that are either differentially expressed or modified, which we call difference-proteins. To characterize this small population of difference-proteins, we have used difference gel electrophoresis [DIGE (Ünlü et al., 1997)] to compare the proteomes of genetically ventralized and lateralized embryos, where most cells in these embryos behave as if they are ventral or lateral cells, respectively. More than 50 difference-proteins were detected. These difference-proteins appeared as the result of increased or decreased abundance and isoform changes resulting from differences in alternative splicing or post-translational modification. Many of these difference-proteins have been identified by mass spectrometry. Seven of the difference-proteins were knocked down by RNAi and all cause ventral furrow defects.

Materials and methods

Fly stocks and embryo collection

The following stocks were used: Tl^{10b}*/TM3/T(1:2)OR60*, snk^{rm4}, Tl^{9Q}*/TM3/T(Y:3)R24* and snk^{073}*/TM3* (kindly provided by Kathryn Anderson) and *Ubi-GFP.nls* (Bloomington Stock Center). Ventralized embryos were collected from Tl^{10b}*/TM3* females that had been mated to snk^{rm4}, Tl^{9Q}/snk^{073} males. Lateralized embryos were collected from snk^{rm4}, Tl^{9Q}/snk^{073} females mated to Tl^{10b}*/TM3* males. snk^{rm4}, Tl^{9Q}/snk^{073} flies were generated by mating snk^{073}*/TM3* females to snk^{rm4}, Tl^{9Q}*/TM3* males.

Embryos were collected on yeasted, apple-juice agar plates over periods of 1-2 hours as described previously (Minden et al., 2000). The embryos were viewed with a dissecting microscope (Wild) using transmitted-light illumination and staged according to Campos-Ortega and Hartenstein (Campos-Ortega and Hartenstein, 1985). Embryos at the desired stage were removed, washed with ethanol, frozen in dry ice and stored at –80°C. Three developmental stages were collected: precellularization (PC) nuclear cycle 11-13, which is 70-100 minutes prior to gastrulation), early gastrulation (EG) 0-10 minutes from the start of gastrulation, and late gastrulation (LG) 10-20 minutes from the start of gastrulation. The start of gastrulation was noted as the first appearance of the cephalic furrow in lateralized embryos and when the basal margin of the cells of ventralized embryos became irregular. For master gel comparisons, embryos were collected for 2 hours and aged for 2 hours at 25°C such that the embryos spanned all three developmental stages from PC to LG.

Difference gel electrophoresis (DIGE)

Typical DIGE gels contained 100 μg of protein for each sample, which is equivalent to about 100 embryos. Protein samples were prepared by pooling the embryos in ethanol into one tube. All transfers were done on dry ice to prevent the embryos from warming above the freezing point. Once sufficient embryos were amassed, they were transferred to a 1.5 ml centrifuge tube that had a fitted plastic pestle, the ethanol was removed and lysis buffer (7 M urea, 2 M thiourea, 4% CHAPS, 10 mM DTT and 10 mM Na-Hepes pH 8.0) was added to 0.5 μl of lysis buffer per embryo, with a maximum of 200 μl per tube. The tube was then transferred to an ice bath and the embryos were homogenized manually with the fitted pestle. This typically yielded a 2 mg/ml protein solution. The protein solutions were labeled with 1 μl of either propyl-Cy3-NHS or methyl-Cy5-NHS – referred to as Cy3 and Cy5, respectively (CyDye DIGE Fluors; Amersham Biosciences) as described previously (Ünlü et al., 1997). Isoelectric focusing was carried out on 13 cm, pH 3-10 non-linear Immobiline strips according to the manufacturer's protocol (Amersham Biosciences). The strips were electrophoresed on an IPGphor apparatus (Amersham Biosciences) for a total of 60-70 kV·hours. After isoelectric focusing, the strips were first equilibrated in a reducing solution containing 2% SDS, 10 mM DTT for 15 minutes at room temperature with gentle swirling and then equilibrated in an alkylating solution containing 2% SDS, 25 mM iodoacetamide and bromophenol blue. The strips were then either immediately loaded on 10-15% SDS-polyacrylamide gradient gels or stored at –80°C. Second dimension electrophoresis was performed at 4°C at a constant current of 10-25 mA per gel.

Gel imaging, image analysis and protein excision

After two-dimensional gel electrophoresis, the gels were removed from the glass plates and fixed in a solution of 40% methanol and 1% acetic acid. Gels were placed in a home-built gel imaging device with an integral gel cutting tool and imaged at two excitation wavelengths (545±10 nm for Cy3 and 635±15 nm for Cy5) using a cooled CCD camera with a 16-bit CCD chip (Roper Scientific). Two separate images for Cy3- and Cy5-labeled proteins were acquired and viewed as a two-frame movie played in a continuous loop. Image manipulation and viewing was done with IPLab Spectrum (Signal Analysis Corp.) and Quicktime (Apple Computer, Inc.) software. Protein differences were detected visually and quantified using an astronomical image analysis software package, SExtractor (Bertin and Arnouts, 1996).

To determine the fold-difference between ventral and lateral expression of a protein, the image fragments were summed to generate a composite image. This summed image was then submitted to SExtractor, which detected the protein spots and created a measurement mask to be applied to the two original image fragments. The mask outlined an area of the gel that contained a protein spot. This was used to define the area in which the pixel values were integrated. The SExtractor program also performed a localized background estimation to determine the base values across the mask area. The output from the image analysis was the sum of pixel values in the mask area less the background sum, which will be referred to as the fluorescence intensity.

Since the overall fluorescence ratio between the dye-labeled proteins is not unity because of the different extinction coefficients of

Cy3 and Cy5 and variation in sample labeling and loading, a normalization factor was determined by averaging the intensity of a set of eight constant regions, which contained a total of 21 protein spots. To aid in balancing the display contrast of the Cy3 and Cy5 images, 1 μg of BSA was added to each protein sample prior to labeling (Fig. 2). The measured intensity ratio for the BSA spots was within one standard deviation (±10%) of the normalization factor.

Proteins of interest were excised from the gel using an automated gel cutter that was an integral component of the fluorescent gel imager, or by hand from Coomassie Blue-stained 2DE (two-dimensional electrophoresis) gels. In-gel tryptic digestion was performed using an Investigator ProGest digester (Genomic Solutions, Ann Arbor, MI) according to the manufacturer's protocol, except that the final extraction was performed using aqueous 0.2% formic acid in place of 0.2% formic acid in acetonitrile. The peptide-containing digest extracts were desalted and concentrated using ZipTip$_{\mu\text{-C18}}$ (Millipore Corp., Bedford, MA) following the manufacturer's instructions.

Protein identification

MS fingerprint analysis was performed on a PerSeptive Biosystems Voyager STR MALDI-TOF instrument operating in the positive ion mode. The range observed was set to 500 – 3000 m/e with 750-1000 scans per spectrum. Each spectrum was processed using Data Explorer (Applied Biosystems). Post-acquistion calibration was performed using the trypsin autolysis products (MH^+ 842.51 and 2211.10) in addition to an added standard (Glu-fibrinogen peptide, 1570.68). Protein identification was done using MASCOT online software [www.matrixscience.com (Perkins et al., 1999)].

Embryo injection and microscopy

Embryos were collected at stage 3 and prepared for micro-injection and time-lapse, fluorescence microscopy as previously described (Minden et al., 2000). Time-lapse microscopy was performed using a Delta Vision microscope system controlled by softWoRx software (Applied Precision, Issaquah, WA) configured around an Olympus IX70 inverted microscope. Time-lapse recordings consisted of 5 optical sections, spaced 2 μm apart, taken at 2 minute intervals over a period of 4 hours. Each image stack was then projected into a single plane and viewed as a time-lapse series of images. Lactacystin was injected as a 5 mM solution in 10% DMF.

dsRNA was synthesized from the following DNA clones (the amplified segments are shown in parentheses, all DNAs were obtained from Research Genetics): twi, BAC clone RPC1-98-8.P.9 (407-1104); sna, BAC clone RPC1-98-23.I.4 (716-1410); pros35, cDNA clone AT04245 (105-598); pros25, cDNA clone RE22680 (5-533); CG17331, cDNA clone GM03626 (7-684); pros29, cDNA clone RE23862 (15-531); bel, cDNA clone RE28061 (11-5720); sqd, cDNA clone LD09691 (104-682); eIF-4e, cDNA clone SD05406 (62-652) and CG3210, cDNA clone GM01975 (13-515). PCR was carried out using primers that contained a T7 promoter sequence on their 5′ ends (TAATACGACTCACTATAGGGAGACCAC). RNA was synthesized using the MEGAscript kit (Ambion) following the manufacturer's instructions. The RNA products were treated with DNaseI for 15 minutes at 37°C and annealed at 65°C for 30 minutes and then allowed to cool slowly at room temperature. The dsRNA was dissolved in injection buffer (Rubin and Spradling, 1982) to a final concentration of not more than 2.5 μM. RT-PCR of dsRNA-injected embryos was performed to confirm the loss of the targeted mRNA.

Results and discussion

Comparison of the proteomes of ventralized and lateralized embryos

Ventral furrow formation is a very rapid process; ventral cells invaginate in about 15 minutes. To understand the cellular changes that occur when ventral cells change their shape during ventral furrow formation, the proteomes of ventral cells and lateral cells were compared. Lateral cells were chosen over dorsal cells because they maintain their columnar shape during gastrulation; dorsal cells adopt a squamous epithelial shape. To obtain relatively pure populations of ventral and lateral cells, genetically ventralized and lateralized embryos were used (St. Johnston and Nüsslein-Volhard, 1992; Ferguson and Anderson, 1992). Females that were heterozygous for Tl^{10b} ($Tl^{10b}/+$) produced ventralized embryos. Females that were heterozygous for Tl^{9Q} ($Tl^{9Q}/+$) and homozygous mutants for *snk* (snk^{073}/snk^{rm4}) produced lateralized embryos. To ensure that the lateralized and ventralized embryos had similar zygotic genotypes, $Tl^{10b}/+$ virgin females were mated to snk^{rm4}, Tl^{9Q}/snk^{073} males to generate ventralized embryos; the reciprocal cross was used to produce lateralized embryos.

To compare the proteomes of ventralized and lateralized embryos, we used DIGE, which is a rapid and sensitive two-dimensional electrophoresis (2DE) method (Fig. 1A). DIGE works as follows. Lysine residues of proteins from whole-embryo homogenates were covalently labeled with either propyl-Cy3 or methyl-Cy5 (referred to as Cy3 and Cy5, respectively). The DIGE dyes were designed to have minimal effect on protein migration during electrophoresis. The Cy3- and Cy5-labeled protein samples were combined and run on the same 2DE gel. After electrophoresis, fluorescence imaging of the 2DE gel with Cy3 and Cy5 excitation light generated two images of the two protein samples in perfect register. Proteins that are common to both samples appear as spots composed of both fluorescent dye molecules. Proteins that are more abundant in one or the other sample appear as spots composed of more of one of the dyes than the other. DIGE is a very sensitive method that can detect as little as 1 fmole of protein and protein differences as low as ±1.2-fold, which is greater than two standard deviations.

We hypothesized that the proteins involved in ventral furrow formation would appear as protein differences between ventral and lateral cells at the time of ventral furrow invagination. Therefore, we compared ventralized embryos to lateralized embryos at three developmental stages: pre-cellularization (PC), early gastrulation (EG) and late gastrulation (LG). In addition to these ventrolateral comparisons, ventralized and lateralized embryos were compared with themselves at different developmental stages. Thus, seven different types of comparisons were performed: three ventrolateral and four temporal (Fig. 1B). Because DIGE is a sensitive method, variation in sample preparation can lead to artifactual differences. To be certain that the difference-proteins reported here were reproducible, all of the comparisons were replicated with independent collections of staged embryos. Six independent ventrolateral comparisons were performed on different embryo collections; the temporal comparisons were done on three independent collections. The findings reported here were from a large collection of staged embryos comprising >400 embryos for each of the six embryo types, and about 100 embryos of each sample were used per comparison. The other independent comparisons showed the same array of protein differences. In addition to this array of comparisons, most of the comparisons were performed in duplicate with reciprocal labeling, such that on one gel sample A was labeled with Cy3 and sample B was labeled with Cy5; the opposite labeling scheme was used for the reciprocal gel.

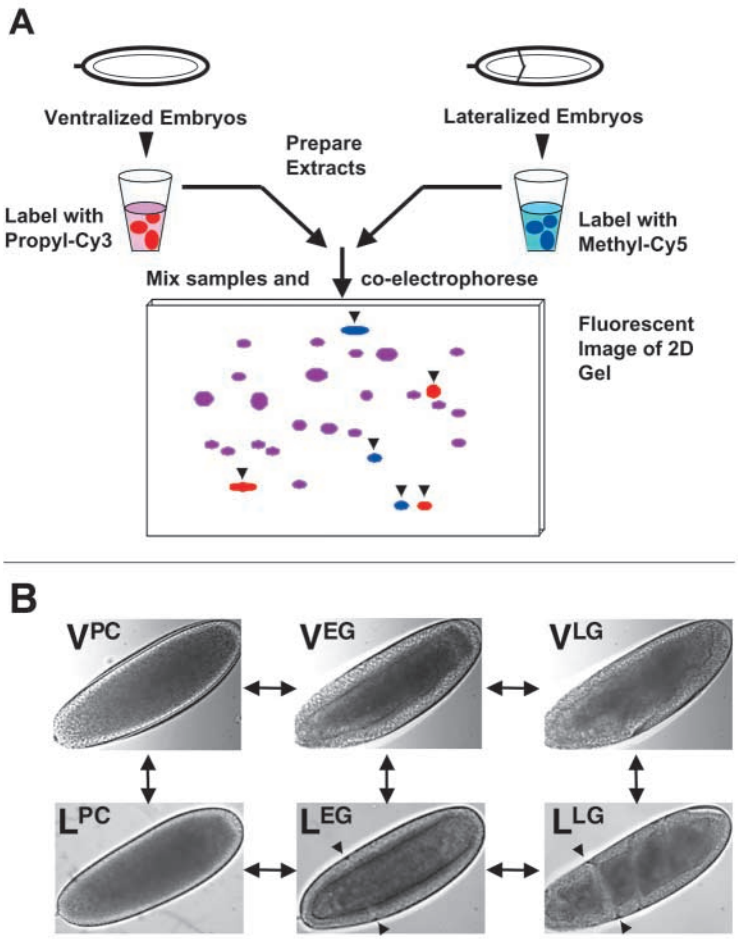

Fig. 1. Difference gel electrophoresis (DIGE) experimental scheme. Collections of ventralized embryos at different developmental stages were compared with lateralized embryos. (A) The general scheme for the DIGE experiments was to prepare whole embryo extracts from ventralized or lateralized embryos. The proteins within each extract were covalently labeled with either propyl-Cy3 or methyl-Cy5. The labeled protein extracts were then combined and co-electrophoresed on a 2DE gel. After electrophoresis, the gel was fixed in methanol and acetic acid and then imaged in the fluorescent gel imaging device at the Cy3 and Cy5 excitation wavelengths. Common protein spots have equal amounts of red-colored Cy3 and blue-colored Cy5, which is shown here as purple. Proteins that are unique to the Cy3-labeled sample are shown as red spots; unique Cy5-labeled proteins are shown as blue spots. (B) Ventralized and lateralized embryos were compared at three developmental stages: pre-cellularization (V^{PC} and L^{PC}), early gastrulation (V^{EG} and L^{EG}) and late gastrulation (V^{LG} and L^{LG}). Shown here are three frames from time-lapse recordings of a ventralized and of a lateralized embryo at the indicated stage. Anterior is to the left. The double-headed arrows indicate the various comparisons that were made. The cephalic furrow is indicated by arrowheads in the L^{EG} and L^{LG} images, the cephalic furrow does not form in ventralized embryos.

To display the full spectrum of protein differences observed in the specific comparisons, master DIGE gels comparing ventralized to lateralized embryos from 2-hour collections spanning all three stages from PC to LG were generated (Fig. 2). Many of the protein changes appeared as protein spots whose abundance varied reciprocally; one protein increased in abundance, while a nearby spot decreased. These reciprocal changes were most probably due to isoform differences resulting from changes in post-translational modification or alternative splicing. To display this phenomenon, difference-proteins are shown as boxed regions that contain multiple protein spots with arrows indicating the proteins that changed. A total of 57 regions are indicated in Fig. 2. The vast majority of the protein changes (55/57 difference regions) were found to be ventrolateral-specific and temporal-independent. Two regions contained proteins that changed in a temporal-specific fashion (Fig. 2, regions T1 and T2). These temporal-specific changes were ventrolateral-independent. Only one region was found to contain a protein that changed in both a ventrolateral- and temporal-specific manner (Fig. 2, region 41). Also shown on the master DIGE gel are: enolase, which was used to determine the relative fluorescent signal of the difference-proteins, BSA, which was added to each labeling reaction as a loading control, and MAPKK, which was used to demonstrate that relatively low abundance proteins are detectable and identifiable on DIGE gels. The two large, dark protein masses are, as indicated, yolk protein clusters.

To view the individual difference-regions more closely, pairs of image sub-fragments showing the ventral and lateral proteins were contrast enhanced and matched (Table 1). These image fragments contained unchanging and changing proteins (difference-proteins are indicated by arrows). In all, 105 difference-proteins were detected from a total of 1315 proteins detected in the master DIGE gel shown in Fig. 2. Of the 105 difference-protein spots, 65 were identified by MS (Tables 1 and 2). The remainder of unidentified protein spots produced insufficient MS spectra because of their low abundance. As mentioned previously, many of the difference-proteins appeared to be isoform changes. This was verified by MS. Thus, a total of 37 unique difference-proteins were identified from the 65 initially identified protein differences. Almost half (18/37) of these difference-proteins appeared to be the result of differential, post-translation modification, while the others appeared to be changes in protein abundance. However, a number of the abundance changes have reciprocally changing neighboring spots that could not be identified by MS. Thus, the ratio of isoform-changes to abundance-changes may be closer to two-thirds. These data indicate that isoform changes appear to play a major role in generating ventrolateral differences. The nature of these changes will be discussed later.

Reproducibility

Two central issues in comparative proteomics analysis are reproducibility and quantification. The main limitation of two-dimensional gel electrophoresis is that no two gels are exactly alike. DIGE alleviates this problem when comparing two or three samples. The data set reported here originated from comparisons between 20 gels: three ventral-lateral comparisons plus their reciprocals (the vertical comparisons in Fig. 1B), four time-dependent comparisons (the horizontal comparisons in Fig. 1B) and 10 master gel comparisons. On average, the protein differences indicated on the master DIGE gel were observed in 16 out of 20 gels. The main reasons for not detecting a

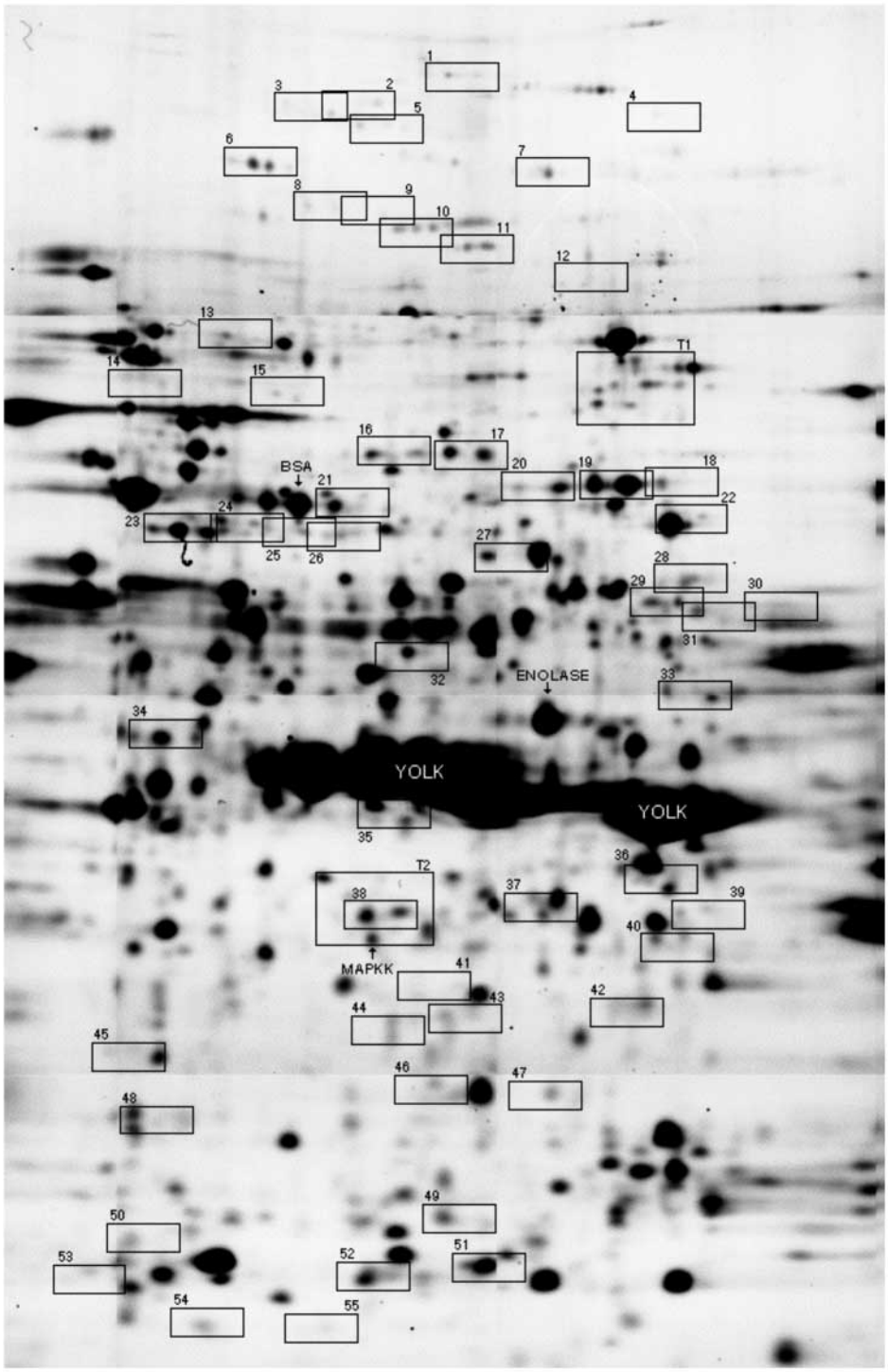

Fig. 2. Master gel comparing ventralized to lateralized embryos. To display the full array of protein differences, collections of ventralized and lateralized embryos spanning the three developmental stages were compared. Shown here is a summed image of the Cy3-labeled lateralized sample and Cy5-labeled ventralized sample. Regions of the gel containing difference-proteins are indicated by numbered boxes. Also shown are unchanging control proteins: BSA (which was added as a loading control), enolase, MAPKK and the two large clusters of yolk proteins.

difference-protein in all gels are poor focusing, which occurs primarily at the gel boundaries, low protein abundance, or a protein residing in a highly crowded region of the gel. All of the difference-proteins reported here were reproducibly detected by DIGE and identified multiple times by MS.

Protein difference quantification

To reliably compare different proteomes, it is essential to measure protein abundance accurately. Digital imaging of fluorescently tagged proteins provides a very high level of accuracy. The fluorescent gel imager used for these studies employed a scientific-grade, cooled CCD camera with a 16-bit CCD chip, which is capable of linearly detecting light over more than four orders of magnitude. The scientific discipline most accustomed to using similar CCD cameras for quantitative image analysis is astronomy. Since at the start of this endeavor there were no commercially available proteomics-oriented gel image analysis software packages capable of dealing with 16-bit images of fluorescently labeled proteins, we adapted an astronomical image analysis package, Source Extractor (referred to as SExtractor), to measure the fluorescence intensity of the protein spots (Bertin and Arnouts, 1996).

Our primary goal for image quantitation was to determine the ratio of ventrally derived proteins relative to laterally derived proteins and to estimate the relative cellular abundance of the difference-proteins. The ratio between a ventral and lateral protein is expressed as fold-difference, where a positive value indicates an excess of ventral protein over lateral protein; a negative value indicates the inverse ratio. Table 1 lists the fold-change for the detected difference-proteins. Over 80% of the difference-proteins could be quantified; the remainder were not detected by the software because of low signal or unresolvable protein spots that were too close to very abundant protein spots. The number of increasing proteins was roughly equal to the decreasing proteins (40:43). These data demonstrate that the vast majority of differences between ventral and lateral cells occur prior to ventral furrow formation. There was no bias in the direction of protein change and only a minority represented absolute on/off changes.

Table 1. Difference-protein regions from the master DIGE gel

Region	Ventral	Lateral	Fold change (ventral:lateral)*	Relative abundance†	*Gene name*, function
1			6.3, –1.6, –1.6	1.8E-2	(a-c) IS
2	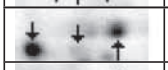		16.7, –1.3, 1.4	7.2E-3	(a-c) IS
3			20.0, 8.3	7.1E-3	(a, b) IS
4			8.3	5.7E-3	IS
5	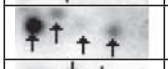	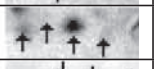	3.1, 6.3, –6.9, 2.2	1.5E-2	(a-d) IS
6			2.0, 2.1, –2.0, –4.8	7.1E-2	(b, c) *Ade2*, Purine biosynthesis (a, d) IS
7	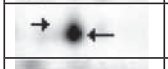		–3.5, 1.5	3.6E-2	(a, b) IS
8	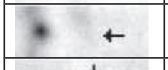		–8.7	5.8E-3‡	IS
9			14.3	4.0E-3	IS
10	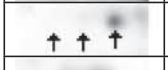	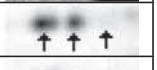	–100, –16.0, 8.3	2.8E-2	(a-c) *CG1516*, Pyruvate carboxylase
11	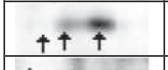		–100, –1.4, 20.0	6.4E-2	(a-c) *CG1516*, Pyruvate carboxylase
12			–100, 3.3	6.6E-3	(a, b) IS
13			2.2	1.3E-2	IS
14		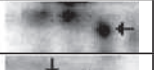	–2.5	3.1E-03	IS
15		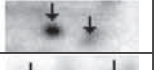	–1.7, 1.5	9.2E-3	(a, b) IS
16			1.9, –2.1	7.0E-3	(a, b) *CG2286*, NADH-ubiquinone reductase
17	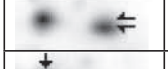		NR	1.0E-1	(a, b) *CG6778*, Glycine-tRNA synthetase
18	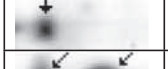		–2.1	3.4E-2	*Tsf1*, Transferrin
19	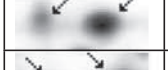		–3.6, –4.1	2.2E-1	(a, b) *Tsf1*, Transferrin
20			–3.0, –4.3	4.0E-2	(a, b) *Tsf1*, Transferrin
21			–100	3.8E-3‡	*ApepP*, Aminopeptidase
22			NR, 2.3	1.8E-2	(a, b) *mRpS30*, Mitochondrial ribosomal protein S30
23			–2.5, 2.2, –5.2	4.0E-1	(a-c) *CG10602*, Leukotriene A4 hydrolase
24			–1.8, NR, NR	9.2E-2	(a-c) IS
25			4.2	4.7E-2	*CG10687*, Asparagine-tRNA synthetase
26			–1.5, 1.2	5.2E-2	(a, b) *CG10687*, Asparagine tRNA synthetase
27			2.0	1.0E-1	*Pgm*, Phosphoglucomutase
28			–1.5	4.2E-2	*CG11208*, Oxalyl-CoA decarboxylase
29			–2.6, 100	3.2E-2	(a, b) *CG4561*, Tyrosine-tRNA synthetase
30			NR, 2.2	1.3E-2	(a) IS (b) *Gdh*, Glutamate dehydrogenase
31			–34.9	3.0E-3‡	*CG5525*, Chaperonin ATPase

Table 1. Continued

Region	Ventral	Lateral	Fold change (ventral:lateral)*	Relative abundance†	*Gene name*, function
32			1.9	1.2E-1	*CG5384*, Ubiquitin-specific protease
33	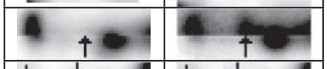		–1.4	5.8E-2	IS
34	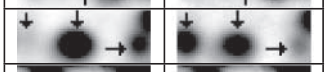		–100, 1.8, 2.1	1.1E-1	(a, b) *CG3731*, Mitochondrial peptidase (c) *Hel25E*, RNA helicase
35			–1.7	2.4E-2	IS
36			NR, NR	ND	(a, b) IS
37			–2.9	1.5E-2	*CG6084*, Aldehyde reductase
38	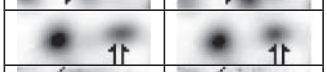		1.1	5.5E-2	(a, b) *CG11980*, Thioredoxin-like protein
39			–10.7, 100	1.3E-2	(a) *Gapdh1* (b) IS
40			1.9, –2.8	7.2E-2	(a) *CG10863*, Aldehyde reductase (b) IS
41			–1.9, NR	3.2E-3	(a) IS (b) *Pros35*, Proteasome α 1 subunit
42			–1.3	1.1E-1	IS
43			1.2	4.0E-2	*RpP0*, Ribosomal protein P0
44			NR	ND	(a-d) *vib*, Phosphatidylinositol transporter
45			–4.0	1.1E-1	IS
46			3.7	2.4E-2	*CG6673*, Glutathione transferase
47			–2.3	1.7E-2	*CG6673*, Glutathione transferase
48			8.3, NR, 7.4, NR	6.8E-2	(a) *CG4265+CG18190*, calponin homology (b) IS (c, d) *CG4265*, Ubiquitin hydrolase
49			–1.2	4.4E-2	*Fer2LCH*, Ferritin *2* light chain homolog
50			–1.4, 100	2.8E-2	(a) IS (b) *Hsp23*, Heat shock protein 23
51			–1.1, 1.5	2.6E-1	(a) *Pros25*, Proteasome α 2 subunit (b) *Pros25 + CG17331*, Proteasome subunit
52			–2.9	3.9E-2	*CG17331*, Proteasome β-type subunit
53			100	7.4E-3	IS
54			2.8	4.9E-2	IS
55			–100	5.7E-3	*twinstar*, Cofilin

Image fragments of boxed regions showing proteins from ventralized and lateralized embryos. Difference-proteins are indicated by arrows. In regions with multiple difference-proteins, the arrows are ordered alphabetically from top-left to bottom-right. The contrast of the master gel image was set to display a number of protein spots similar to that of a silver-stained gel. However, many of the rectangles in the master gel appear to be empty. This is because the proteins within these spots are in low abundance and the contrast of the image was insufficient to display the proteins. If the overall contrast was increased to display these proteins, the higher abundant protein spots would coalesce into large dark masses of indistinguishable spots, like that of the yolk proteins.

*The fold change of ventral/lateral protein signal. The maximum reported fold-change is 100, the actual value may be greater .

†Relative abundance using the most abundant difference from the ventralized sample.

‡Relative abundance using the most abundant difference from the lateralized sample.

NR, not resolved; ND, not determined; IS, insufficient MS signal.

Table 2. MS identification of difference-proteins

Gel region	Gene name*	Molecular function	Mascot score†	Seq. cov. (%)‡	Mol mass (Da)§	pI
Metabolic enzymes						
6b,c	*ade2*	Purine biosynthesis	227	22	149641	5.48
10a-c, 11a-c	*CG1516*	Pyruvate carboxylase	125	20	131522	6.37
16a,b	*CG2286*	NADH:ubiquinone reductase	206	34	79493	6.43
27	*Pgm*	Phosphoglucomutase	84	17	61114	6.25
28	*CG11208*	Oxalyl-CoA decarboxylase	103	20	62795	7.16
30b	*Gdh*	Glutamate dehydrogenase	88	15	61340	8.44
37	*CG6084*	Aldehyde reductase	103	21	36185	6.21
38	*CG11980*	Thioredoxin-like protein	155	39	36210	5.97
39a	*Gapdh1*	Glyceraldehyde-3-phosphate dehydrogenase	65	21	35465	8.26
40a	*CG10863*	Aldehyde reductase	145	43	36689	6.60
Proteases						
21	ApepP	Aminopeptidase	69	16	68862	5.63
23a-c	*CG10602*	Leukotriene-A4 hydrolase	66	13	68959	5.32
32	*CG5384*	Ubiquitin-specific protease	108	24	54129	5.93
34a,b	*CG3731*	Mitochondrial processing peptidase	98	23	52525	5.67
41b	*Pros35*	Proteasome 35kD α-type1 subunit	214	58	31211	6.09
48c,d	*CG4265*	Ubiquitin carboxy-terminal hydrolase	98	40	26005	5.31
51a,b	*Pros25*	Proteasome 25kD α-type1 subunit	184	51	26004	6.21
51b,52	*CG17331*	Proteasome β-type2 subunit	80	42	22524	5.95
Iron metabolism						
18, 19a,b, 20a,b	Tsf1	Transferrin 1	334	47	72963	6.89
49	*Fer2LCH*	Ferritin 2 light chain homologue	108	51	25489	5.90
Cytoskeleton						
31	*CG5525*	Chaperonin ATPase	206	32	57117	7.50
48a	*CG18190*	Calponin-homology domain, EB1-domain	67	15	27152	5.48
50b	*Hsp23*	Heat shock protein 23	89	51	20616	5.55
55	*tsr*	Cofilin	143	52	17428	6.74
RNA-binding proteins						
22a,b	*mRpS30*	Mitochondrial ribosomal protein S30	135	26	65238	8.53
34c	*Hel25E*	RNA helicase	67	18	49077	5.43
43	*RpPO*	Ribosomal protein P0	103	30	34295	6.48
T1b	*belle*	RNA helicase	184	25	85371	7.18
T2a	*sqd*	Squid RNA-binding protein	134	31	35039	6.16
T2b	*CG4035*	eIF-4E, Eukaryotic initiation factor 4E	90	41	27924	5.22
tRNA synthetases						
17a,b	*CG6778*	Glycine-tRNA synthetase	96	16	76554	6.02
25, 26a,b	*CG10687*	Asparagine-tRNA synthetase	100	26	64462	5.69
29a,b	*CG4561*	Tyrosine-tRNA ligase	93	18	58408	6.42
Membrane-associated proteins						
23a-c	*CG10602*	leukotriene-A4 hydrolase	66	13	68959	5.32
44a-d	*vib*	Phosphatidylinositol transporter	116	36	31495	5.61
T1a,c	*CG3210*	Dynamin-like protein	69	12	83085	6.51
Miscellaneous						
46, 47	*CG6673*	Glutathione transferase	148	40	28764	6.54

*FlyBase entry (http://flybase.bio.indiana.edu/).
†Scores >57 are considered significant (Perkins et al., 1999).
‡Seq. cov., sequence coverage.
§Molecular mass includes all lysines as modified carbamidomethyl-lysine.

The fluorescent gel imager has a linear detection range of over 10,000-fold. To demonstrate the concentration range of difference-proteins detected, the intensity of the most abundant difference-protein per region was calculated relative to enolase, which is a high abundance, constant protein (Table 1). The difference-proteins occurred over a wide concentration range from 4×10^{-3} (region 9) to 0.4 (region 23) of the enolase signal. It is not possible to provide an absolute measure of protein abundance since we do not know the exact correlation between fluorescence signal and the amount of a particular protein. These values should be considered as estimates since the exact stoichiometry of labeling may vary slightly from protein to protein. This small variation in individual protein labeling characteristics does not lead to variability in difference detection as evidenced by earlier experiments (Ünlü et al., 1997; Tonge et al., 2001).

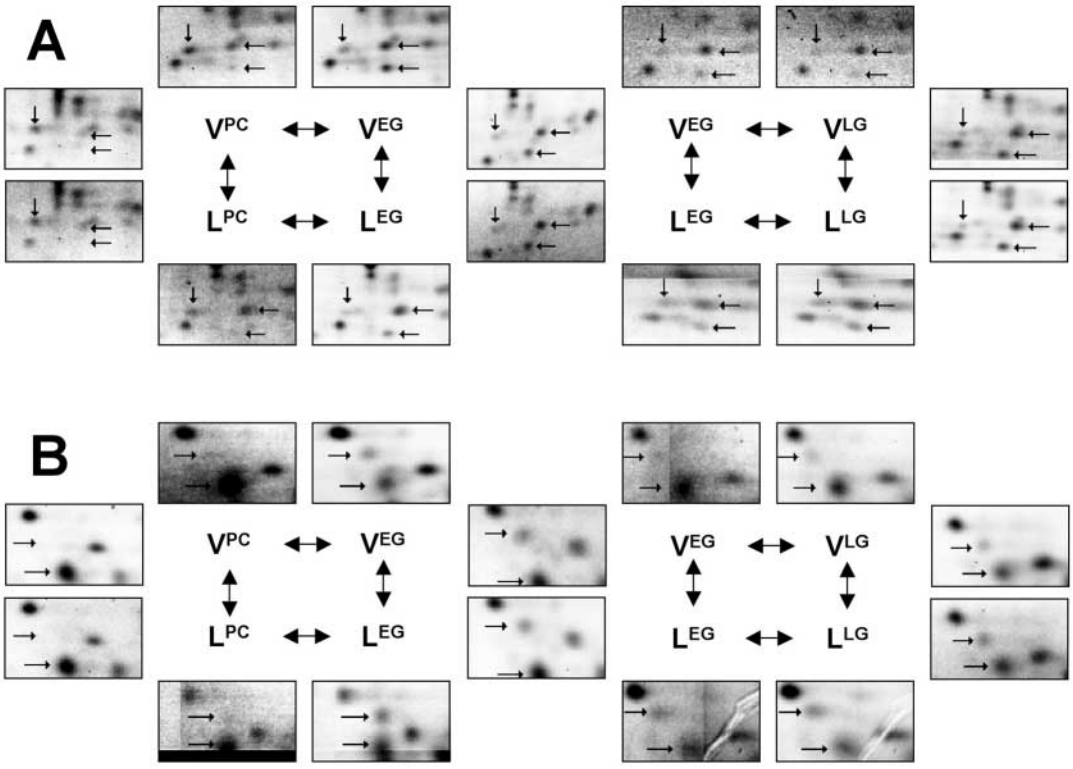

Fig. 3. Temporal-specific protein differences. To show the dynamic behavior of the temporal-specific difference proteins, image fragments from the various comparisons are displayed. The difference-proteins are indicated by arrows. (A) Difference-proteins in the T1 region. Notice the decrease of T1a (top-left spot) in both V^{EG} and L^{EG} images and the corresponding increase of T1b (top-right spot) and T1c (lower-right spot). (B) Difference proteins in the T2 region. Notice the increase of T2a (upper spot) in both V^{EG} and L^{EG} images and the decrease of T2b (lower spot).

Classes of difference-proteins

As stated above, there are two general classes of protein changes: abundance and isoform changes. Abundance changes can be the result of changes in the rate of synthesis or rate of degradation. Isoform changes may be due to alternative splicing or post-translational modification. Post-translational modification generally alters the isoelectric point of a protein (pI). Phosphorylation, myristylation and methylation make proteins more acidic, causing a leftward shift on 2DE gels; esterification makes proteins more basic, causing a rightward shift. Some modifications, such as glycosylation and prenylation, alter the molecular weight of proteins. Proteolysis can change both the pI and molecular mass of a protein. We have seen examples of shifts in protein location in all possible directions. MS analysis for some proteins, such as pyruvate caboxylase (regions 10 and 11), NADH-ubiquinone reductase (region 16) and leukotriene-A4 hydrolase (region 23), indicated differential phosphorylation. Larger quantities of these proteins will be required to precisely determine the nature of their phosphorylation differences. Some proteins exhibited complex changes. Leukotriene-A4 hydrolase (region 23) and asparagine tRNA synthetase (regions 25 and 26) were detected as three isoforms with the central isoform increasing at the expense of the flanking isoforms. This behavior suggests that these proteins are undergoing multiple molecular changes. These results show that isoform changes are likely to play a significant role in ventrolateral specification since over half of all differences are isoform changes.

Temporal-specific protein changes

The vast majority of protein changes appeared in all ventrolateral comparisons regardless of the developmental stage. There were, however, three regions that contained proteins that changed between pre-cellularization and early gastrulation and remained constant over late gastrulation (Fig. 2, 41b, T1 and T2 regions, and Fig. 3). The protein changes in two of these regions (T1 and T2) appeared to be independent of ventral or lateral specification; while the third region (41b) contained a protein that changed both temporally and spatially.

Three difference-protein spots occurred within the T1 region, T1a-c (Fig. 3A). T1a decreased upon gastrulation and remained low both ventrally and laterally. T1b and T1c increased at gastrulation and remained elevated. T1b changed modestly with an increase of 30% and T1c increased more than threefold. T1a and T1c were both identified as CG3210, a dynamin-like protein. T1b was identified as Belle, a DEAD box containing an ATP-dependent, RNA helicase that is closely related to Vasa and is implicated in translation initiation and RNP nuclear export (Lasko, 2000).

Two temporal-specific changes were found in the T2 region. T2a increased upon gastrulation, while T2b decreased. Both experienced greater than threefold changes that did not show any ventrolateral specificity. T2a was identified as Squid, a protein required for mRNA localization. Squid was originally discovered as an RNA-binding protein required for dorsoventral axis formation (Kelly, 1993; Matunis et al., 1994). T2b was identified as eIF-4E, which binds directly to the mRNA 5′-cap and has been shown to accumulate in the mesoderm (Hernández et al., 1997). The role of four of these time-dependant proteins in ventral furrow formation was investigated further and is shown in a subsequent section.

The only difference-protein to show both ventrolateral and temporal specificity was region 41b, which was identified as PROS35, an α1 proteasome subunit. Previous analysis of PROS35 showed that it accumulates in the ventral furrow

(Haass et al., 1989). Unfortunately, the antibody used in these studies has since been lost. The PROS35 difference-protein spot was located just to the left of a moderately abundant, unchanging protein that was also identified as PROS35. These two proteins spot were so closely associated in the master gel that they could not be resolved by SExtractor (Fig. 2, region 41). The nature of the acidic shift of PROS35 is not known. The limited number of temporal-specific changes indicates that our original hypothesis regarding the mechanics of ventral formation needs to be re-examined.

Synopsis of difference-proteins

One of the main reasons for using a proteomics approach to analyze ventral furrow morphogenesis was to identify new proteins involved in this complex process. The MS-identified difference-proteins fell into several distinct categories, which are lists in Table 2. The two most highly represented groups of proteins were metabolic enzymes and proteases, with ten and eight candidates, respectively. A preponderance (7 of 10) of the metabolic enzymes are involved in redox reactions, many of which utilize NAD or flavin co-factors. This may indicate that ventral and lateral cells have different energy requirements and different metabolic or oxidative states.

Further indication of the different metabolic states of ventral and lateral cells is the changing levels of two iron-carrying proteins: transferrin 1 (Tsf1), and ferritin 2 light chain homolog, FER2LCH, both of which are reduced in ventral cells. The majority of cellular iron is found in the mitochondria where it is required for redox reactions. Differences in iron-transport proteins and several mitochondrial proteins involved in redox reactions suggest clear metabolic differences between ventral and lateral cells.

Proteases make up the second largest group of difference-proteins, with eight members. Three are proteasome subunits and two are ubiquitin hydrolases showing that proteasome-dependent degradation may play a role in ventral furrow formation. The remaining three are involved in modifying amino termini, which may also affect protein stability. All three of the proteasome subunit changes appear to be isoform changes. It is not possible to determine the functional state or capabilities of the different isoforms without further biochemical analysis. Additional rounds of DIGE and other biochemical experiments will be required to determine the substrates for these proteases and their ultimate role in ventral furrow formation. Further analysis of the role of the proteasome is presented in the following section.

Cell shape changes most probably involve cytoskeletal changes. Three of the difference-proteins are known to interact with the cytoskeleton. Cofilin, which is decreasing in ventral cells, is a well-known actin binding protein required for destabilizing the cortical actin network (Svitkina and Borisy, 1999). Hsp23 has been shown to have an actin binding homology domain (Goldstein and Gunawardena, 2000). CG18190 appears to interact with actin filaments through a calponin homology domain (Korenbaum and Rivero, 2002) and with microtubules through an EB1 domain (Tirnauer and Bierer, 2000).

In addition to the cytoskeletal associated proteins, we detected a change in a member of the T-complex chaperonin, CG5525, which is a homologue of CCT4. The T-complex chaperonin is involved in folding newly synthesized α- and β-tubulin and actin. This may indicate different actin and tubulin turnover rates in ventral and lateral cells. The levels of actin and tubulin appear to be constant. It is reasonable to expect the turnover rate of cytoskeletal proteins to change during cell shape modulation. Perhaps the cyto-architecture is being altered by coupling local proteolysis to the synthesis of new cytoskeletal elements elsewhere in the cell.

Three of the difference-proteins were tRNA synthetases (RS): tyr-RS, gly-RS and asn-RS, all three RS differences were seen as isoform changes. RSs are generally thought of as housekeeping genes. However, the expression of specific RSs appears to be developmentally regulated in a tissue-specific manner in *Drosophila* embryos (Seshaiah and Andrews, 1999). During mammalian apoptosis, tyr-RS has been shown to be cleaved to generate two different cytokines (Wakasugi and Schimmel, 1999). Further experiments are required to test if tyr-RS is acting as a cytokine during ventral furrow formation.

In addition to cytoskeletal changes, one might expect membrane changes during ventral furrow formation. Three of the difference-proteins are associated with membrane changes. Leukotriene-A4 hydrolase functions in leukotriene B4 biosynthesis from arachadonic acid. Leukotrienes are known to stimulate cell migration during inflammation (Ford-Hutchinson, 1990). The phosphatidylinositol transporter, Vibrator (Vib), was seen as two, vertical spots that were shifted upward in molecular mass in ventral cells (Table 1, spot 44). Vib has been implicated in both actin-based processes and signal transduction and is used repeatedly throughout development (Spana and Perrimon, 1999). The third membrane-associated difference-protein is CG3210, a dynamin-like protein that shows a temporal-specific, isoform change. Dynamin is a GTPase involved in the pinching off of membrane vesicles. Dynamin-like proteins have also been implicated in mitochondrial membrane fusion and plant cell cytokinesis and polarity (McQuibban et al., 2003; Kang et al., 2003). Clearly, *vib* and *CG3210* will require further investigation to determine their link to ventral furrow formation.

Validating the role of the proteasome in ventral furrow morphogenesis

Three of the ventrolateral-specific changes were in proteasome subunits. To explore the role of these proteins in ventral furrow formation, the proteasome was inhibited by drug treatment and RNA interference. Ventral furrow formation was monitored by time-lapse, fluorescence microscopy of embryos ubiquitously expressing nuclear localized GFP (*Ubi-GFP.nls*). In wild-type embryos, ventral cells invaginate rapidly; the furrow was visible within 4 minutes of the end of cellularization and completed about 12 minutes later (Fig. 4, column A). Injection of the proteasome inhibitor, lactacystin, into syncytial-stage embryos caused a pronounced delay in ventral furrow formation. A modest furrow first appeared 20 minutes after the end of cellularization and was completed 80 minutes later (Fig. 4, column B). To gauge the lactacystin effect, RNAi against *twi* and *sna* was done. *twi* and *sna* are transcription factors that cause ventral furrow defects when mutated. Embryos that are mutant for both *twi* and *sna* completely fail to form a ventral furrow. Injection of dsRNA against both *twi* and *sna* caused a range of defects from mild, with delayed furrow formation,

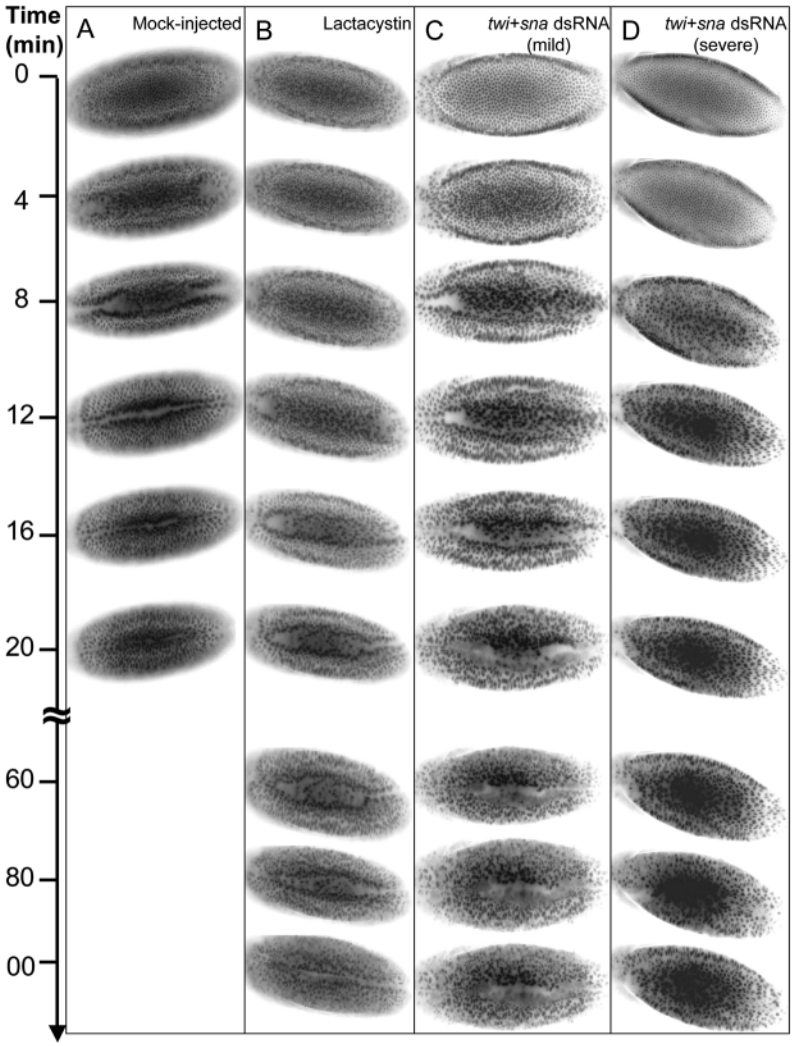

Fig. 4. Lactacystin inhibition of ventral furrow formation. Time-lapse microscopy of ventrally-oriented *Ubi-GFP.nls* embryos. (A) Images from a time-lapse recording of a mock-injected embryo. (B) Images from a time-lapse recording of an embryo injected with lactacystin. (C) Images from a time-lapse recording of an embryo injected with dsRNA to *twi* and *sna*. Shown here is an example of a mildly defective ventral furrow. (D) Images from a time-lapse recording of an embryo injected with dsRNA to *twi* and *sna*. Shown here is an example of a severely defective ventral furrow.

(Fig. 4, column C) to severe, with a complete inhibition of furrow formation (Fig. 4, column D). The lactacystin-injected embryo shown in Fig. 4 suffered a mild ventral furrow defect. The distribution of mild to severe ventral furrow defects is plotted in Fig. 5. The overall percentage of defects was similar for *twi* and *sna* RNAi alone or in combination. The main difference was that *twi* and *sna* together had a slightly higher fraction of severe defects. Lactacystin was not as potent as the *twi* + *sna* RNAi.

Lactacystin is a general proteasome inhibitor, but it may interact with other proteins in the embryo. To determine the role of the proteasome subunits identified as difference-proteins, we used RNAi to reduce the expression of *pros25*, *pros35* and *CG17331* alone or in combination (Fig. 5). Injection of dsRNA of these three genes individually lead to ventral furrow defects that were similar in severity and extent as RNAi of *twi* or *sna* alone. Combinations of dsRNA species that included *pros35* increased the severity by about 75%. Combining *CG17331* and *pros25* did not increase the fraction of severe ventral furrow defects. These results indicate that *pros25* and *CG17331* may have redundant functions and that *pros35* with either *pros25* or *CG17331* have nearly additive effects on ventral furrow morphogenesis. Two control injections were performed. Mock injections of buffer caused a limited number of injection-related defects. Injection of dsRNA of a proteasome subunit that was not a difference-protein, *pros29*, only yielded a small percentage of mild ventral furrow defects. These data clearly demonstrate that the proteasome is indeed involved in ventral furrow morphogenesis. A curious link between ventral furrow formation and the immune system is the observation of the immunoproteasome, which is a derivative of the proteasome involved in antigen presentation, that has several subunit changes (Tanaka, 1994; Preckel et al., 1999). This version of the proteasome is particularly sensitive to lactacystin. Lactacystin was the only one of several proteasome inhibitors tested that caused ventral furrow defects (data not shown). It will be very interesting to discover the targets of the ventral-specific proteasome.

Validating the role of time-dependent difference proteins in ventral furrow morphogenesis

Four temporal-specific difference proteins were chosen as targets for RNAi in an attempt to elucidate their roles in ventral furrow formation. dsRNA was synthesized against *belle* (*bel*), squid (*sqd*), *eIF-4e* and CG3210 and injected into syncytial-stage embryos. Reducing the levels of all these proteins led to defects in ventral furrow morphogenesis, albeit showing different levels of severity (Fig. 5). Inhibiting *bel* resulted in low levels of ventral furrow defects; this can be attributed to the small change in levels of Bel at gastrulation. Inhibition of all the other genes led to ventral furrow defects similar to those seen before. As before, mock injections performed with only buffer resulted in extremely low levels of defects. It is interesting to note that even though there were fewer temporal-specific changes seen than expected, all time-dependent proteins tested seem to play an important role in some aspect of ventral furrow formation, since reducing their levels in embryos leads to defects in ventral furrow morphogenesis. It remains to be determined why the timing of appearance of these proteins is critical in controlling changes associated with ventral furrow formation.

Concluding remarks

It is curious that the majority of ventrolateral-specific changes are stage independent and that all but one of the temporal-specific changes are ventrolateral independent. Only PROS35 was found to be both ventrolateral- and temporal-specific for

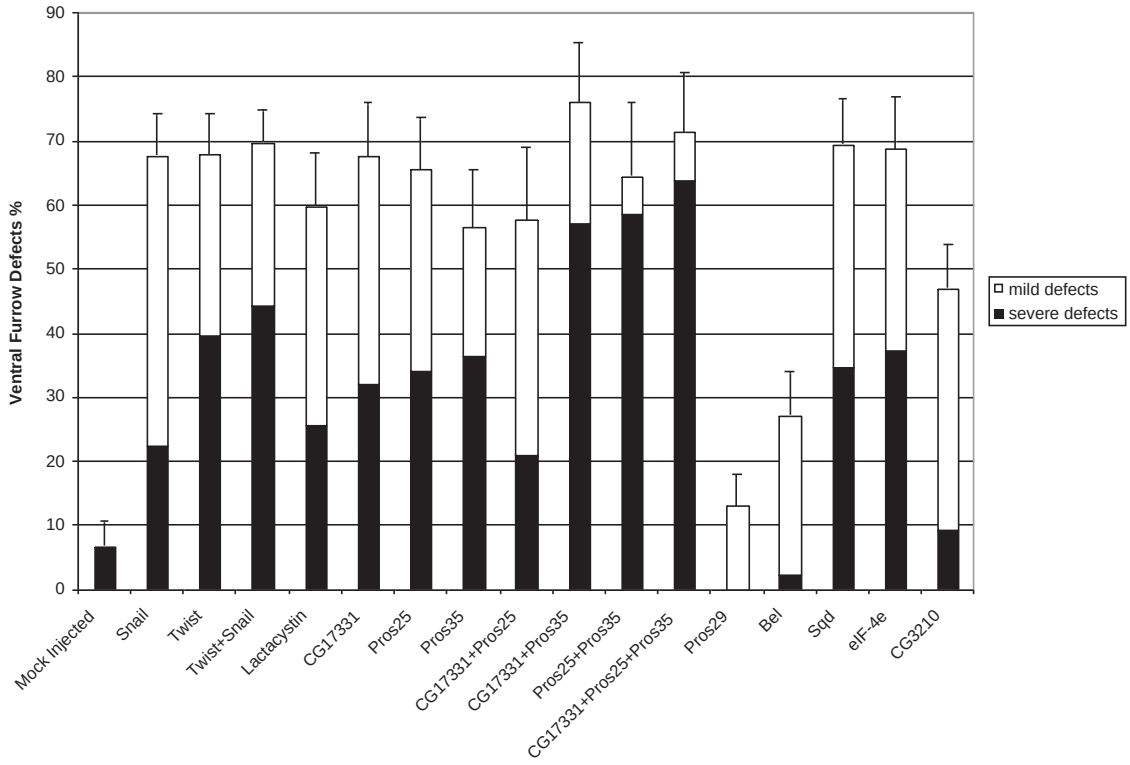

Fig. 5. RNAi of proteasome subunits and time-dependant difference proteins interferes with ventral furrow morphogenesis. Time-lapse analysis of ventrally oriented *Ubi-GFP.nls* embryos injected with dsRNA of several difference proteins. Data is presented as a histogram plot of the percentage ventral furrow defects upon injection of different dsRNAs alone or in various combinations. Bars indicate s.d.

ventral furrow formation. Our findings indicate that the ventral side of the embryo is primed for the cell shape changes associated with ventral furrow morphogenesis during the syncytial blastoderm stage. Initially, we had anticipated that most of the protein changes would coincide with ventral furrow formation. It is possible that such a class of proteins might either not be resolved by 2DE or be below the detection level of the fluorescence imager. Our results show that of the ventrolateral-specific differences, there was a 32:1 ratio of temporal-independent to temporal-dependent protein changes. Increasing the resolution and sensitivity of 2DE is not likely to alter this ratio radically. It is reasonable to assume that most of the protein differences that specify ventral cells occur well before gastrulation. It is well established that the dorsoventral signaling components are activated during the syncytial blastoderm stage. Dorsal is nuclear localized as early as nuclear cycle 10 (Steward, 1989; Roth et al., 1989); nuclear Twist is also evident by nuclear cycle 13 (Thisse et al., 1988). There are limits to DIGE protein detection and MS identification of proteins isolated from 2DE gels. Neither Twist nor Snail has been identified in the ventrolateral comparisons. These are low abundance, transcription factors that are difficult to accumulate in sufficient amounts for MS identification. Over half of the difference-proteins represent isoform changes. The only class of modifying enzymes identified were proteases; no kinases were identified as difference-proteins. Further biochemical characterization of the isoform differences will provide clues to the identity of the modifying proteins.

Two previous studies of transcript differences between ventralized and lateralized embryos revealed a number of ventral-specific transcripts [nine novel ventral genes (Casal and Leptin, 1996); 19 novel ventral genes (Stathopoulos et al., 2002)]. None of these gene products were identified in this proteome analysis. It could be argued that the abundance of the differentially expressed gene products was too low for MS identification. Several studies have demonstrated that there is no direct correlation between transcript level and protein level (Anderson and Seilhamer, 1997; Gygi et al., 1999). One of the most highly changing transcripts was found to be actin57B, which is a major cytoskeletal component in the embryo (Stathopoulos et al., 2002). Actin is a highly abundant, well resolved protein on 2DE gels. We did not observe any changes in actin abundance in the ventrolateral comparisons. The reason for this discrepancy is not clear. Perhaps the gene is transcribed, but not translated or there is increased protein turnover holding the actin level at a steady state. Understanding the relationship between mRNA and protein levels will surely provide additional insight into this process.

What, then, triggers the formation of the ventral furrow? We propose that the ventral cells are primed to change shape at the completion of cellularization. Prior to basal closure at the end of cellularization, the ventral cytoskeletal components are poised to perform the apical constriction, but the gross morphological changes cannot occur without individual cells. Upon completion of cellularization, the cytoskeleton is able to deform the surface of the newly formed ventral cells, precipitating ventral furrow morphogenesis. It would be interesting to block cellularization without perturbing the hexagonal arrangement of nuclei and determine if ventral furrow formation is also blocked. The four temporal-specific

difference-proteins that have no ventrolateral-specificity, may provide insight into the process of cellularization. Clearly there is much more work to be done. Comparative proteomics should be viewed as a starting point in an investigative cycle that, with other experimental manipulations, can help to uncover the network of functions and interactions required for a variety of developmental process. Our studies have shown that in addition to cell signaling, transcriptional regulation, cytoskeletal changes and cell cycle regulation, ventral furrow morphogenesis also involves translational control, protein degradation, membrane alterations and metabolic changes, demonstrating that morphogenesis is a complex process that encompasses nearly all cellular processes.

We would like to thank Chuck Ettensohn, Adam Linstedt and the Minden lab for their critical reading of the manuscript, and Kathryn Anderson and the Bloomington Stock Center for fly stocks. This work was supported by a grant from the National Institutes of Health (GM62274) to J.S.M.

References

Anderson, L. and Seilhamer, J. (1997). A comparison of selected mRNA and protein abundances in human liver. *Electrophoresis* **18**, 533-537.

Bertin, E. and Arnouts, S. (1996). SExtractor: software for source extraction. *Astronomy and Astrophysics* **117**, 393-404.

Boulay, J. L., Dennefeld, C. and Alberga, A. (1987). The *Drosophila* developmental gene *snail* encodes a protein with nucleic acid binding fingers. *Nature* **330**, 395-398.

Campus-Ortega, J. A. and Hartenstein, V. (1985). Stages of *Drosophila* embryogenesis. In *The Embryonic Development of* Drosophila melanogaster, pp. 9-84. Berlin: Springer-Verlag.

Casal, J. and Leptin, M. (1996). Identification of novel genes in *Drosophila* reveals the complex regulation of early gene activity in the mesoderm. *Proc. Natl. Acad. Sci. USA* **93**, 10327-10332.

Chou, T. B. and Perrimon, N. (1996). The Autosomal FLP-DFS technique for generating germline mosaics in *Drosophila melanogaster*. *Genetics* **144**, 1673-1679.

Costa, M., Sweeton, D. and Wieschaus, E. (1993). Gastrulation in *Drosophila*: cellular mechanisms of morphogenetic movements. In *The Development of* Drosophila melanogaster (ed. M. Bate and A. Martinez Arias), pp. 425-465. Cold Spring Harbor, New York: Cold Spring Harbor Laboratory Press.

Costa, M., Wilson, E. T. and Wieschaus, E. (1994). A putative cell signal encoded by the *folded gastrulation* gene coordinates cell shape changes during *Drosophila* gastrulation. *Cell* **76**, 1075-1089.

Ferguson, E. L. and Anderson, K. V. (1992). *decapentaplegic* acts as a morphogen to organize dorsal-ventral pattern in the *Drosophila* embryo. *Cell* **71**, 451-461.

Ford-Hutchinson, A. W. (1990). Leukotriene B4 in inflammation. *Crit. Rev. Immunol.* **10**, 1, 1-12.

Goldstein, L. S. and Gunawardena, S. (2000). Flying through the *Drosophila* cytoskeletal genome. *J. Cell Biol.* **150**, F63-F68.

González-Crespo, S. and Levine, M. (1993). Interactions between DORSAL and helix-loop-helix proteins initiate the differentiation of the embryonic mesoderm and neuroectoderm in *Drosophila*. *Genes Dev.* **7**, 1703-1713.

Grosshans, J. and Wieschaus, E. (2000). A genetic link between morphogenesis and cell division during formation of the ventral furrow in *Drosophila*. *Cell* **101**, 523-531.

Gygi, S. P., Rochon, Y., Franza, B. R. and Aebersold, R. (1999). Correlation between protein and mRNA abundance in yeast. *Mol. Cell. Biol.* **19**, 1720-1730.

Haass, C., Pesold-Hurt, B., Multhaup, G., Beyreuther, K. and Kloetzel, P. M. (1989). The PROS-35 gene encodes the 35 kd protein subunit of *Drosophila melanogaster* proteasome. *EMBO J.* **8**, 2373-2379.

Hall, A. (1998). Rho GTPases and the actin cytoskeleton. *Science* **279**, 509-514.

Hernández, G., Diez del Corral, R., Santoyo, J., Campuzano, S. and Sierra, J. M. (1997). Localization, structure and expression of the gene for translation initiation factor eIF-4E from *Drosophila melanogaster*. *Mol. Gen. Genet.* **253**, 624-633.

Kam, Z., Minden, J. S., Agard, D. A., Sedat, J. W. and Leptin, M. (1991). *Drosophila* gastrulation: analysis of cell shape changes in living embryos by three-dimensional fluorescence microscopy. *Development* **112**, 365-370.

Kang, B. H., Busse, J. S. and Bednarek, S. Y. (2003). Members of the Arabidopsis dynamin-like gene family, ADL1, are essential for plant cytokinesis and polarized cell growth. *Plant Cell* **15**, 899-913.

Kelley, R. L. (1993). Initial organization of the *Drosophila* dorsoventral axis depends on an RNA-binding protein encoded by the squid gene. *Genes Dev.* **7**, 948-960.

Korenbaum, E. and Rivero, F. (2002). Calponin homology domains at a glance. *J. Cell Sci.* **115**, 3543-3545.

Lasko, P. (2000). The *Drosophila melanogaster* genome: translation factors and RNA binding proteins. *J. Cell Biol.* **150**, F51-F56.

Leptin, M. (1991). TWIST and SNAIL as positive and negative regulators during *Drosophila* mesoderm development. *Genes Dev.* **5**, 1568-1576.

Leptin, M. and Grunewald, B. (1990). Cell shape changes during gastrulation in *Drosophila*. *Development* **110**, 73-84.

Mata, J., Curado, S., Ephrussi, A. and Rorth, P. (2000). Tribbles coordinates mitosis and morphogenesis in *Drosophila* by regulating string/CDC25 proteolysis. *Cell* **101**, 511-522.

Matunis, E. L., Kelley, R. and Dreyfuss, G. (1994). Essential role for a heterogeneous nuclear ribonucleoprotein (hnRNP) in oogenesis: hrp40 is absent from the germ line in the dorsoventral mutant squid. *Proc. Natl. Acad. Sci. USA* **91**, 2781-2784.

McQuibban, G. A., Saurya, S. and Freeman, M. (2003). Mitochondrial membrane remodeling regulated by a conserved rhomboid protease. *Nature* **423**, 537-541.

Minden, J. S., Namba, R. and Cambridge, S. (2000). Photoactivated gene expression for cell-fate mapping and cell manipulation. In *Drosophila protocols* (ed. W. Sullivan, M. Ashburner and R. S. Hawley), pp 413-427. Cold Spring Harbor, New York: Cold Spring Harbor Laboratory Press.

Parks, S. and Wieschaus, E. (1991). The *Drosophila* gastrulation gene *concertina* encodes a Gα-like protein. *Cell* **64**, 447-458.

Perkins, D. N., Pappin, D. J., Creasy, D. M. and Cottrell, J. S. (1999). Probability-based protein identification by searching sequence databases using mass spectrometry data. *Electrophoresis* **20**, 3551-3567.

Perrimon, N., Lanjuin, A., Arnold, C. and Noll, E. (1996). Zygotic lethal mutations with maternal effect phenotypes in *Drosophila melanogaster*. ii. Loci on the second and third chromosomes identified by P-element-induced mutations. *Genetics* **144**, 1681-1692.

Preckel, T., Fung-Leung, W. P., Cai, Z., Vitiello, A., Salter-Cid, L., Winqvist, O., Wolfe, T. G., Von Herrath, M., Angulo, A., Ghazal, P. et al. (1999). Impaired immunoproteasome assembly and immune responses in PA28–/– mice. *Science* **286**, 2162-2165.

Roth, S., Stein, D. and Nüsslein-Volhard, C. (1989). A gradient of nuclear localization of the *dorsal* protein determines dorsoventral pattern in the *Drosophila* embryo. *Cell* **59**, 1189-1202.

Rubin, G. M. and Spradling, A. C. (1982). Genetic transformation of *Drosophila* with transposable element vectors. *Science* **218**, 348-353.

Santaren, J. (1990). Towards establishing a protein database of *Drosophila*. *Electrophoresis* **11**, 254-267.

Seher, T. C. and Leptin, M. (2000). Tribbles, a cell-cycle brake that coordinates proliferation and morphogenesis during *Drosophila* gastrulation. *Curr. Biol.* **10**, 623-629.

Seshaiah, P. and Andrews, D. J. (1999). WRS-85D: a tryptophanyl-tRNA synthetase expressed to high levels in the developing *Drosophila* salivary gland. *Mol. Biol. Cell* **10**, 1595-1608.

Spana, E. and Perrimon, N. (1999). The vibrator gene encodes a phosphatidylinositol transfer protein and is required for the acquisition and execution of cell fate. *A. Dros. Res. Conf.* **40**, 368A.

St. Johnston, D. and Nüsslein-Volhard, C. (1992). The origin of pattern and polarity in the *Drosophila* embryo. *Cell* **68**, 201-219.

Stathopoulos, A., Van Drenth, M., Erives, A., Markstein, M. and Levine, M. (2002). Whole-genome analysis of dorsal-ventral patterning in the *Drosophila* embryo. *Cell* **111**, 687-701.

Steward, R. (1989). Relocalization of the *dorsal* protein from the cytoplasm to the nucleus correlates with its function. *Cell* **59**, 1179-1188.

Svitkina, T. M. and Borisy, G. G. (1999). Arp2/3 complex and actin depolymerizing factor/cofilin in dendritic organization and treadmilling of actin filament array in lamellipodia. *J. Cell Biol.* **145**, 1009-1026.

Sweeton, D., Parks, S., Costa, M. and Wieschaus, E. (1991). Gastrulation

in *Drosophila*: the formation of the ventral furrow and posterior midgut invaginations. *Development* **112**, 775-789.

Tanaka, K. (1994). Role of proteasomes modified by interferon-gamma in antigen processing. *J. Leukoc. Biol.* **56**, 571-575.

Thisse, B., Stoetzel, C., Gorostiza, T. C. and Perrin-Schmitt, F. (1988). Sequence of the *twist* gene and nuclear localization of its protein in endomesodermal cells of early *Drosophila* embryos. *EMBO J.* **7**, 2175-2183.

Tirnauer, J. S. and Bierer, B. E. (2000). EB1 proteins regulate microtubule dynamics, cell polarity, and chromosome stability. *J. Cell Biol.* **149**, 761-766.

Tonge, R., Shaw, J., Middleton, B., Rowlinson, R., Rayner, S., Young, J., Pognan, F., Hawkins, E., Currie, I. and Davison, M. (2001). Validation and development of fluorescence two-dimensional differential gel electrophoresis proteomics technology. *Proteomics* **1**, 377-396.

Ünlü, M, Morgan, M. E. and Minden, J. S. (1997). Difference gel electrophoresis: a single gel method for detecting protein changes in cell extracts. *Electrophoresis* **18**, 2071-2077.

Wakasugi, K. and Schimmel, P. (1999). Two distinct cytokines released from human aminoacyl-tRNA synthetase. *Science* **284**, 147-151.

Young, P. E., Pesacreta, T. C. and Kiehart, D. P. (1991). Dynamic changes in the distribution of cytoplasmic myosin during *Drosophila* embryogenesis. *Development* **111**, 1-14.